

MODELLING REGIONAL SCALE SURFACE ENERGY EXCHANGES AND CBL GROWTH IN A HETEROGENEOUS, URBAN-RURAL LANDSCAPE

H. A. CLEUGH¹ and C. S. B. GRIMMOND²

¹*CSIRO Land and Water, Pye Laboratory, PO Box 1666, Canberra ACT 2601, Australia;*

²*Atmospheric Science Program, Department of Geography, Indiana University, Bloomington, IN 47405, U.S.A.*

(Received in final form 9 June 2000)

Abstract. Over the last decade, simple models of the convective boundary layer (CBL) have been suggested as an approach to inferring regionally averaged land-air exchanges of heat, water and trace gases, because the properties of the CBL respond to an average of the underlying small-scale heterogeneity. This paper explores the use of an integral CBL method to infer regionally averaged fluxes in a landscape that has at least three major sources of heterogeneity – irrigated and non-irrigated rural land use and a large urban area (Sacramento region, California).

The first part of the paper assesses the validity of the simple slab model of the CBL – this is integrated forwards in time using local-scale measured heat and water vapour fluxes, to predict mixed-layer depth, temperature and humidity. Of the four different CBL growth schemes used, the Tennekes and Driedonks model is found to give the best performance. Evaluation of the model performance with different weightings of heat and water vapour fluxes based on the land use characteristics in the region suggest that the source area for the boundary-layer sonde measurements is larger than physically-based estimates would suggest.

Finally, measured time series of potential temperature are used to infer regionally averaged sensible heat fluxes using an integral CBL (ICBL) method. These ICBL fluxes are compared with those measured at the local scale over the three land use types that comprise the region of interest. They are found to be closest to the heat fluxes calculated by appropriately weighting the measured heat fluxes in the source area calculated for the ICBL. We conclude that the integral CBL budget method provides adequate estimates of regionally-averaged surface heat fluxes in a landscape that is characterised by surface types with distinctly different surface energy budgets.

Keywords: CBL budget methods, CBL (convective boundary layer), Microscale heterogeneity, Regional fluxes.

1. Introduction

A current challenge in boundary-layer meteorology is to provide, either through modelling or measurements, estimates of turbulent fluxes that are representative of large regions, covering areas of 10^2 – 10^4 km², where the landscape is inevitably characterised by considerable surface heterogeneity. We define this larger area as the ‘regional scale’ in this paper. Examples of applications where such information is in demand include monitoring regional scale carbon, water and nutrient budgets for the purpose of assessing and managing landscape sustainability, quantifying



greenhouse gas budgets and managing water resources. While current technology and theoretical understanding enable the direct measurement of turbulent fluxes that are representative of the field or local scale (i.e., averaging over areas *ca.* 10^4 m²), alternative approaches are required to determine spatially integrated fluxes over these much larger regions. Such alternatives include aircraft, tall towers, or the development of appropriate models. Simple models of the convective boundary layer (CBL), because of the averaging properties of the CBL, offer a method of spatial integration. Several studies, primarily conducted in agricultural landscapes, have estimated regional-scale exchanges of heat, water vapour and trace gases using CBL budget methods, e.g., Brutsaert and Mawdsley (1976), Munley and Hippias (1990), Cleugh (1991), and Culf (1992). The studies by Raupach et al. (1992), Denmead et al. (1996), and Cleugh et al. (1997) demonstrate the viability of using such methods to determine spatially averaged scalar fluxes in heterogeneous landscapes.

In this paper we explore the use of CBL methods to infer regionally averaged fluxes in a landscape with three distinct land uses (irrigated, non-irrigated rural and urban) that lead to spatially variable surface moisture, roughness, thermal, and radiative properties. This work makes a contribution beyond the earlier studies by assessing the validity of CBL budget methods in a landscape that exhibits much more extreme surface heterogeneity, at a range of horizontal length scales, and for which we have information about the nature of the surface heterogeneity.

2. Surface Fluxes: Relationship between Direct Measurements and Boundary-Layer Budget Estimates

2.1. THE ATMOSPHERIC BOUNDARY LAYER: FLUXES AND CONCENTRATIONS

The surface-atmosphere exchange of entities such as heat, water and trace gases can be determined by directly measuring the vertical turbulent flux of that entity using fast response sensors located in the surface layer. The horizontal length scale of the flux source area, which can be estimated using a variety of source area or footprint models (e.g., Leclerc and Thurtell, 1990; Schmid and Oke, 1990; Horst and Weil, 1992; Schmid, 1994, 1997) is of order 0.1–1 km, depending on sensor height and atmospheric turbulence. The horizontal length scale of both the source area, and the individual sources within, must form the basis for any assessment of the representativeness of a turbulent flux measurement (Schmid, 1997). Most tower-based direct flux measurements do not provide regionally averaged surface-atmosphere exchanges, because their source areas are usually local scale (0.01–1 km²). The flux measurements will also not be representative in heterogeneous landscapes where the horizontal length scale of the surface heterogeneity approaches or exceeds the turbulence flux source area. For these reasons, approaches have been developed that infer regionally averaged fluxes from a time series of scalar concentrations or velocities in the atmospheric boundary layer (ABL). These approaches, collectively termed ‘ABL budget methods’, exploit the spatial averaging properties of the

ABL. They have the advantage of representing larger source areas as well as only needing, in principle, concentration rather than turbulent flux measurements.

This study focuses on the convectively dominated ABL, the CBL, which develops under conditions typical of stable, anticyclonic weather – clear skies, high solar radiation and light winds. The relationship between surface-layer turbulent flux measurements and CBL-derived fluxes is presented in Section 2.2 where CBL structure, characteristic response times and length scales and approximate dimensions of ABL source areas are considered. Section 2.3 briefly describes the CBL above a city, because the region used in this study encompasses both rural and urban land uses.

2.2. DESCRIPTION AND MODEL OF THE DAYTIME CBL

The vertical structure of a well-developed CBL includes a relatively shallow surface layer where scalar concentration and velocity gradients are large, and a well-mixed layer where convective turbulence and strong mixing limits the development of vertical concentration gradients. The upper limit of this well-mixed layer (z_i) is marked by a potential temperature inversion where convective turbulence is reduced. Within this upper region the potential temperature (θ) gradient, defined as γ_θ , indicates the strength of the inversion. Similarly, the humidity (q) gradient above the CBL is denoted as γ_q .

Figure 1 illustrates the typical diurnal evolution of potential temperature and humidity in and above the CBL. These measured profiles, which were acquired in this study (see below), accord very well with the theoretical structure portrayed in the literature (e.g., Cleugh, 1991; Raupach et al., 1992; Denmead et al., 1996). The CBL grows from sunrise as sensible heating encroaches and eventually erodes the nocturnal radiation inversion. The CBL grows rapidly through the preceding day's well-mixed layer that forms a residual or fossil layer above the radiation inversion. Convective plumes with vertical velocities of $1\text{--}2\text{ m s}^{-1}$ ascend through the CBL, sometimes overshooting and penetrating into the capping inversion. Once in this stable layer, their negative buoyancy forces them to sink back down into the CBL and in so doing the turbulent kinetic energy and temperature of the CBL is increased. This entrainment of warm, dry air from aloft further warms the mixed layer and produces a discontinuity in the vertical gradients of potential temperature and humidity. Thus an entrainment zone lies at the interface between the mixed layer and the free atmosphere which is often parameterised as a 'jump' or a 'step' in zero-order mixed-layer growth models (the so-called slab model, described below). In fact, observations using lidar show that the depth of the entrainment zone may be up to 20% of the CBL depth (Cooper and Eichinger, 1994).

This structure and diurnal development of the CBL forms the basis of a simple predictive CBL model, the 'slab model', the basic equations for which are well established. The CBL is represented as a well-mixed layer, overlying a thin surface layer and capped by a potential temperature inversion as illustrated in Figure 1. The

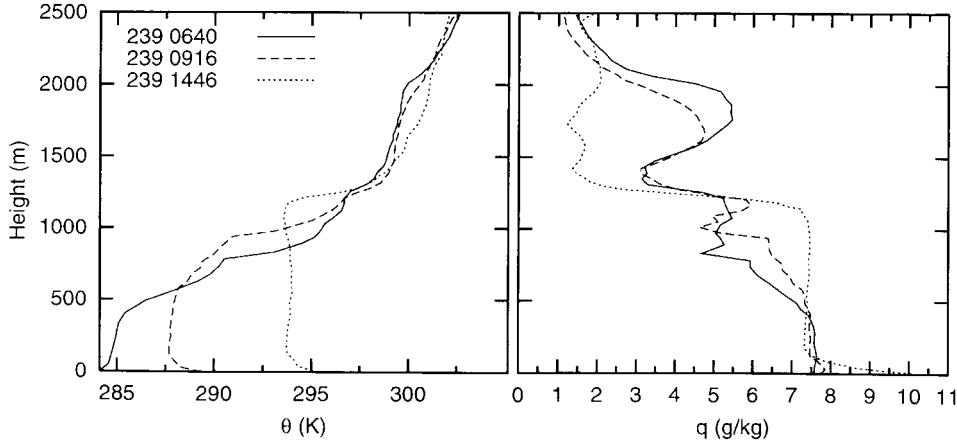


Figure 1. Example of typical temperature and humidity profiles in the CBL Sacramento, Day 91/239.

appropriate conservation equations for heat and water vapour, assumed to be well mixed within the CBL and expressed in a semi-Lagrangian form (see Raupach, 2000), are:

$$\frac{d\theta_m}{dt} = \frac{\partial F_H}{\partial z} = \frac{F_{HO}}{z_i} + \frac{\theta_+ - \theta_m}{z_i} \left[\frac{dz_i}{dt} - w_s \right], \quad (1)$$

$$\frac{dq_m}{dt} = \frac{\partial F_E}{\partial z} = \frac{F_{EO}}{z_i} + \frac{q_+ - q_m}{z_i} \left[\frac{dz_i}{dt} - w_s \right], \quad (2)$$

where $d/dt = \partial/\partial t + U\partial/\partial x$; θ_m and q_m are the potential temperature and specific humidity in the well-mixed portion of the CBL; F_H and F_E are the kinematic sensible and latent heat fluxes ($Q_H/\rho c_p$ and Q_E/L_v , respectively), and F_{HO} and F_{EO} are the *surface* fluxes; z_i is the CBL depth; θ_+ and q_+ are the potential temperature and specific humidity immediately above z_i , and w_s is the subsidence velocity. The net flux across the capping inversion is given by the second term on the RHS, *viz* $[(\theta_+ - \theta_m)(dz_i/dt - w_s)]$ in the case of heat. The concentration ‘jump’ across the inversion ($\theta_+ - \theta_m$, $q_+ - q_m$) is often written as $\Delta\theta$ and Δq for heat and water vapour, respectively. Essentially Equations (1) and (2) show that scalar concentrations within the CBL are determined by the scalar fluxes at the surface, entrainment of free air from aloft, and subsidence.

Solving Equations (1) and (2) requires a model for the growth of the CBL, which must include both entrainment and encroachment mechanisms. The most commonly used equations are:

McNaughton and Spriggs (1986) encroachment:

$$\frac{dz_i}{dt} = \frac{F_{Hv}}{z_i \gamma \theta_v}. \quad (3a)$$

Tennekes and Driedonks (1981) entrainment:

$$\frac{dz_i}{dt} = \frac{(\alpha_1 w_*^3) + (\alpha_2 u_*^3)}{z_i \Delta\theta_v g \theta_v^{-1}}. \quad (3b)$$

Tennekes (1973) entrainment:

$$\frac{dz_i}{dt} = \frac{\alpha_3 F_{Hv}}{\Delta\theta_v}. \quad (3c)$$

Rayner and Watson (1991) entrainment:

$$\frac{dz_i}{dt} = \frac{\alpha_4 w_*^3 + (\alpha_5 u_*)^3}{\alpha_6 [\alpha_4 w_*^3 + (\alpha_5 u_*)^3]^{2/3} + [z_i \Delta\theta_v g \theta_v^{-1}]}, \quad (3d)$$

where g is the acceleration due to gravity; α_i are constants; u_* and w_* are the friction and convective velocities; F_{Hv} is the virtual heat flux ($[Q_H + 0.07Q_E]/\rho c_p$) and (γ_{θ_v} , $\Delta\theta_v$, and θ_v are as defined above, but use virtual potential temperature. The three entrainment models (b–d) range from a simple estimate of the size of the heat flux at z_i (c), to the more complex expressions, (b) and (d), which parameterise the influence of both shear-driven and convective turbulence on entrainment. The value of α_3 is typically taken to be 0.2 (e.g., Tennekes, 1973) but evidence from studies at lower (subtropical) latitudes with high convective activity suggest that 0.5 may be a more appropriate value for α_3 (Cleugh et al., 1997). The values for α_i , including an appropriate value for α_3 , are discussed in greater detail later.

In summary, the inputs required to solve Equations (1)–(3) to predict the time rate of change of z_i , θ_m and q_m , are: the surface heat and water vapour flux; initial CBL depth and scalar concentration (z_{io} ; θ_{mo} and q_{mo}); and the gradient of heat (γ_θ) and humidity (γ_q) and their respective concentrations (θ_+ , q_+) above z_i . It is worth noting that practical application of this slab model using CBL profiles measured using radiosondes is often limited in two important ways. Firstly, estimating θ_+ , q_+ from instantaneous sonde profiles is very difficult and, secondly, such measurements are Eulerian. This means that advection (the $U d/dx$ term implicit in Equations (1) and (2)) is assumed to be negligible or must be diagnosed from synoptic maps or model output.

The scalar budget equations can also be used to infer the surface fluxes, F_{HO} and F_{EO} (see Raupach et al., 1992; Denmead et al., 1996), using a measurement of $d\theta_m/dt$ and dq_m/dt together with dz_i/dt (either measured or modelled). We define this approach, following the suggestion of M. R. Raupach (personal communication), as the DCBL method (differential CBL method) for inferring surface fluxes. Such an approach has been used by, for example, Munley and Hipps (1990) to infer surface evaporation fluxes at a prairie grassland site. Note that such an approach requires adequate time resolution, i.e., $d/dt < 1$ h, to enable an accurate estimate of $d\theta_m/dt$ or dq_m/dt .

This definition differentiates the DCBL approach from the integral CBL (ICBL) methods whose basic equation results from integrating the conservation equation through time. For a scalar with concentration S , assumed well-mixed through the mixed layer and with a surface flux F_{SO} , the following expression (see Tennekes, 1973) results:

$$\int_{t_i}^{t_{i+1}} F_{SO} dt = \frac{\gamma_s}{2} [z_i(t_{i+1})^2 - z_i(t_i)^2] - [(z_i, \Delta S)_{t_{i+1}} - (z_i, \Delta S)_{t_i}] + \int_{t_i}^{t_{i+1}} \overline{w_s} \Delta S dt, \quad (4)$$

where t_i and t_{i+1} are used to denote values at two consecutive time periods. The integration time (dt , see below) is therefore the time period over which the ICBL equation is applied. Raupach et al. (1992), Cleugh and Grimmond (1993), Denmead et al. (1996) and others have used various forms of this integral equation to estimate time and space-integrated exchanges of heat, water vapour and CO_2 between the land surface and the atmosphere.

Following Raupach (1991), we can argue on both physical and dimensional grounds that the distance required (X) for CBL properties to adjust to a change in surface flux is related to z_i , U (the mean horizontal wind speed in the mixed layer), and the convective velocity scale, w_* :

$$X = \frac{z_i U}{w_*}, \quad (5)$$

where w_* is:

$$w_* = \left(\frac{g F_{Hv} z_i}{\theta_v} \right)^{1/3}. \quad (6)$$

The convective time scale, $t_* = X/U = z_i/w_*$, is the time taken for a surface signal to reach the capping inversion, *ca.* 10–30 min, and is sometimes referred to as the eddy turnover time. The CBL will be fully mixed over time scales that are long compared to t_* .

Scalar concentrations in the CBL represent an average of the underlying surface heterogeneity, with a characteristic horizontal length scale of l_s , providing $l_s \ll X$. Raupach (1991) referred to this as ‘microscale’ heterogeneity, and argued that CBL scalar concentrations reflect the areally averaged fluxes of these scalars to/from the underlying surface in these situations. An equivalent statement is that the CBL will be fully mixed over length scales greater than Ut_* and l_s thus needs to be much less than $Ut_*(X)$ in order for CBL scale averaging to occur.

Figure 2a,b shows relationships between z_i , X and t_* , respectively, for different wind speeds and sensible heat fluxes, and thus convective velocity (as w_* depends

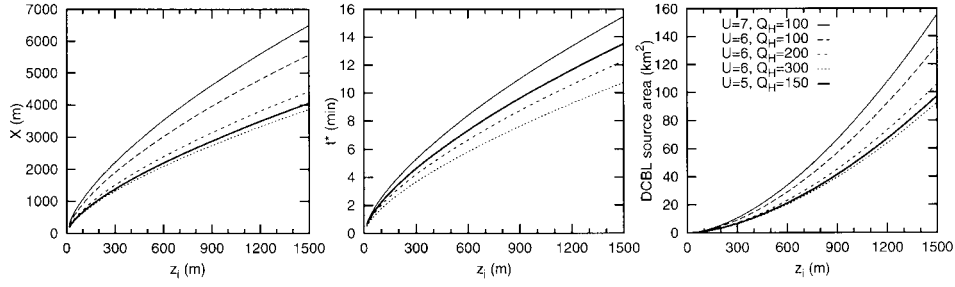


Figure 2. Variation of X , t_* and DCBL source area for varying CBL depth; CBL wind speed (U), and heat fluxes (Q_H) (see text for equations). Note that the 2 curves for $Q_H = 100 \text{ W m}^{-2}$ in the middle panel are coincident.

primarily on z_i and F_{HO}). For typical CBL depths, X varies from 1–6 km, and t_* from 8–16 min. It is clear from Figure 2 that the length scale X depends very much on the relative strength of the horizontal mean wind speed and the convective velocity. X , and hence t_* , become smaller when the convective velocity scale exceeds the mean horizontal wind speed.

To reiterate, if the length scale of the characteristic heterogeneity (l_s) is small in comparison to the length scale for CBL adjustment (X), then CBL scalar concentrations are an average of all the scalar sources in the landscape underlying the CBL. Miao and Cleugh (1997), using a mesoscale model (RAMS, Pielke et al., 1992) found that the upper limit for microscale heterogeneity corresponded to l_s of about 10 km. Mesoscale heterogeneity, and associated CBL-scale advection, occurs when $l_s \gg X$. In these situations, a one-dimensional slab model, such as described in Equations (1)–(3), may not be appropriate.

An order of magnitude estimate for the size of the source area for a CBL scalar concentration, and thus the source area for the flux (F_{SO}) can be determined for either the differential (i.e., Equations (1)–(3)) or the integral (Equation (4)) approaches. Considering the former and using the arguments above, M. R. Raupach (personal communication) suggests an expression for the CBL source area that is based on a length scale equivalent of four ‘eddy turnover times’ (i.e., $4X$) – the time scale over which the CBL can be considered to be fully mixed:

$$SA_{\text{DCBL}} = \left[\frac{U}{w_*} \right] 16z_i^2. \quad (7)$$

Under typical conditions, Equation (7) gives a source area of around 10–100 km² (see Figure 2c) and a length scale of 3–10 km. This is an order of magnitude estimate of the dimensions of the source area that influences the time rate of change of a CBL scalar concentration, given a surface scalar flux F_{SO} . Thus, if a detailed time series of S has been measured (to yield dS/dt) then we might imagine that the surface flux, F_{SO} , is averaged over a source area with these dimensions. Equation

(7) thus provides an estimate of the averaging area for a flux inferred by the DCBL method.

If integral CBL methods, e.g., Equation (4), are used to infer surface fluxes, as attempted in this study, a slightly different expression for the averaging area is required because Equations (1)–(2) are typically integrated over long time periods. A very simple estimate can be determined by considering, in convective conditions, that a typical travel distance for an air parcel in the CBL is Ut , where t is the integration time ($t_{i+1} - t_i$ in Equation (4)) and that this must be roughly similar to the length scale of this averaging area. An alternative expression to this simple estimate suggested by M. R. Raupach (personal communication) is:

$$SA_{\text{ICBL}} = Uw_*t^2, \quad (8)$$

which yields averaging areas that are of similar order to Ut . Under typical convective conditions, the predicted averaging area is *ca.* 1000 km² for an integration time of 6 h. In other words CBL scalar concentrations are in equilibrium with scalar fluxes from an area whose dimensions, roughly 30 × 30 km, are about 1–2 orders of magnitude larger than the source area for fluxes inferred from the DCBL method. Most landscapes have significant spatial heterogeneity at these length scales. The possible need to consider the advective terms in the CBL budget equation is a potential dilemma if integral methods are adopted to estimate regional scale surface fluxes.

Nonetheless, more and more studies are using ICBL methods to infer regional scale heat, water vapour and CO₂ fluxes. Several, e.g., Lhomme et al. (1997), Culf (1992), Hipps et al. (1994), found that such methods provided reasonable estimates of regional sensible heat fluxes, but performed poorly for water vapour and CO₂ exchanges. The careful approach taken by Betts and collaborators (e.g., Barr and Betts, 1997; Barr et al., 1997), where the absence of mesoscale advection was confirmed through measurements and modelling and ensemble CBL profiles used, illustrates that the ICBL method can provide very accurate estimates of regional scale exchanges. Their results from the FIFE experiment (Betts and Ball, 1994), where advection was determined from model analyses, also show that CBL budget methods perform well if the advective terms are explicitly included.

2.3. THE CBL ABOVE A CITY

The region in this study comprises three main land cover types: irrigated rural; unirrigated rural and urban. In addition, the foothills to the east of the city are forested. More details about the attributes of these land cover types are given below, here we focus on urban land use and in particular the CBL above urban areas.

A city is characterised by a complex array of surface types with varying radiative, thermal and aerodynamic properties. This extreme urban surface heterogeneity has horizontal length scales that range from the dimensions of an individual building through to city blocks, land use zones, up to the size of the city as a whole.

The largest scale of heterogeneity, the horizontal dimensions of the entire city, may be much greater than the traditional microscale heterogeneous length scale as defined by Raupach (1991). If we consider ‘urban’ as a single land use, then a city may be classed in the category of mesoscale heterogeneity. Placing urban land use into the class of mesoscale heterogeneity has two important implications. Firstly, mesoscale circulations may develop as a result of differences in surface energy exchanges between the city and the surrounding rural land use. In these cases the averaging ideas presented above may no longer hold. Miao and Cleugh (1997) find that mesoscale circulations may prevent CBL ‘smoothing’ if the convective available potential energy is large and there is a strong contrast in surface heating between the city and its surroundings. Secondly, both microscale and mesoscale advection may be common in cities (Oke, 1976; Godowitch et al., 1987) as a result of spatial variations in surface energy exchanges at both the microscale (1–100 m) and the typical horizontal length scale of a land use zone (1–10 km).

As air is advected over a city, dS/dt will be influenced by the city within a few Ut_* – i.e., 1–5 km or 15–30 min – after the air moves past the city’s leading edge. Where the upwind extent of a city is larger than ca. 10 km, given the averaging arguments presented above, the time rate of change of CBL scalar concentrations will be averaged over, and thus represent, solely urban land use. Forward predictions of CBL depth and scalar concentrations using the slab model (Equations (1)–(3)) should thus be forced using an *urban* heat flux. If integral (ICBL) methods are used, the inferred surface fluxes may be averaged over trajectories that extend more than 50 km upwind of the site where boundary layer profiles are made. Except for cities with a large spatial extent, the underlying urban and the surrounding non-urban land use will both influence these fluxes.

3. Objectives

The previous section has outlined the theoretical basis for using CBL budget methods to infer surface fluxes averaged over areas with length dimensions varying from <10 km (DCBL) to 50 km (ICBL). Such approaches have promised much because of their ability to spatially average surface heterogeneity and because the only inputs required are fairly straightforward concentration measurements. Thus far, however, the few published applications of CBL budget methods have focussed on agricultural or ‘natural’ (unmanaged) landscapes where the surface heterogeneity is not extreme. Furthermore, these studies have not investigated the nature of the heterogeneity introduced by different land surface types, or had measurements of the local-scale fluxes above each of these land surfaces. In short, there is a pressing need for further evaluation of such techniques, especially in landscapes exhibiting large spatial heterogeneity.

The overall aim of this study is to exploit the detailed energy balance measurements for the three different land uses comprising the Sacramento region, described

in Grimmond et al. (1993), to further evaluate CBL budget methods and to assess the source, or averaging area, for the surface fluxes inferred from these methods. It goes beyond past studies by including urban and rural land uses, with a range of horizontal length scales of heterogeneity, and by carefully evaluating CBL budget methods through the following four steps:

1. Integrate the slab model forwards in time, using Equations (1)–(3) and measured surface heat and water vapour fluxes, to predict mixed-layer depth, temperature and humidity. This analysis evaluates the applicability of the slab model for the CBL above a city, determines the importance of measurement error and identifies a suitable entrainment scheme. Poor performance of the CBL model at this step would mean that attempts to *infer* fluxes using such a model would be fruitless.
2. The DCBL method cannot be used to infer surface fluxes because the temporal resolution, which is only 2 h at best, of the CBL scalar concentration time series is inadequate. Rather we explore the sensitivity of the forward predictions of $d\theta/dt$ and dq/dt to changing measures of the ‘regional’ surface heat and water vapour flux to infer the appropriate source area. This step thus determines the most appropriate heat and water vapour flux with which to force the slab model and evaluate its applicability. It is an indirect way of inferring the appropriate source area for the DCBL method.
3. Use measured CBL scalar concentrations to infer spatially-averaged surface fluxes using the *integral* CBL method.
4. Compare the fluxes determined in (3) with those individual fluxes measured over each of the land use types in the region, and with a ‘regional’ flux. The latter is calculated by weighting the individual fluxes measured over each land use type by the fraction of the source area made up of that land surface type. This enables an assessment of both the ICBL method and the source area expressions for this and the DCBL methods.

Section 4 briefly describes the measurement program (details are provided in Grimmond et al., 1993) while Section 5 presents an analysis of the land-use in the region of interest and a description of the CBL structure for the study period. Sections 6 and 7 present the results from Steps 1 to 4. Section 8 discusses the results and the important conclusions.

4. Measurement Program

4.1. STUDY AREA

A field program was conducted in the vicinity of Sacramento (38°39' N, 121°30' W), within the Sacramento–San Joaquin valley, California, U.S.A. (Figure 3). The Sacramento metropolitan area has a population of 1.48 million and is surrounded by intensive agricultural land use. Instruments were installed at three sites to char-

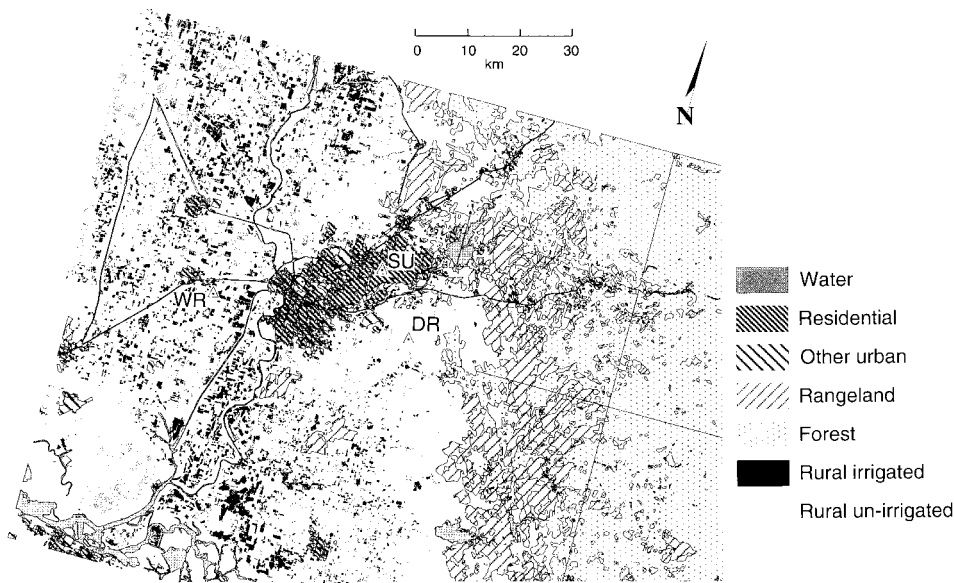


Figure 3. Location of study sites and land use in the region. Sources used: <http://edcwww.cr.usgs.gov/glis/hyper/guide/1char95250lulc>, January 23, 1998 <http://www.biogeog.ucsb.edu/projects/gap/gapchar95data.html>, February 5, 1998.

acterise the surface energy balance of the three predominant land use types in the region (Figure 3):

- (a) *Dry rural (DR)*: located 18.1 km southeast of downtown Sacramento, with a surface cover of long (approximately 0.5 m), non-irrigated grass.
- (b) *Wet rural (WR)*: located in an extensive irrigated grass farm approximately 17.7 km to the southwest of downtown Sacramento.
- (c) *Suburban (SU)*: located in a school playing field in the residential neighbourhood of Carmichael, 16.6 km northeast of the downtown area. Instruments were placed at sufficient height (28.5 m) to measure local scale fluxes representative of the land use in the suburb – predominantly single storey, single family dwellings with well-irrigated (mesicape) vegetation.

The topography within the vicinity of all the sites is generally flat. The Sacramento–San Joaquin valley runs NW–SE with the Sierra Nevada Mountain range to the east and the Coastal Range to the west. Sacramento is located on the eastern side of the valley, which is approximately 80 km wide in this area. Sacramento is 150 km from the Pacific Ocean and air can penetrate through the break in the Coastal Range in the San Francisco Bay area. The region has a mesothermal Mediterranean-type climate, with a hot dry summer. The average near-surface air temperature in August 1991 was 22.9 °C, slightly lower than the normal, and only 0.25 mm of rain was recorded in the six weeks prior to the measurement period. The general synoptic conditions for the measurement period were typical for the

area, with an anticyclone located off the West Coast of California, and predominantly westerly winds. A cold front crossed southern Oregon/Idaho on August 24th (designated day 91/236) and extended into Northern California on August 25th (91/237). A second front, which had previously been stationary over southern Oregon, passed through the Sacramento region on August 28th (91/240). During the period of observations the sky conditions were clear, with occasional night cloud.

4.2. OBSERVATIONS

Sensible and latent heat fluxes were measured at each site using the eddy correlation approach and using a Campbell Scientific (CSI) one dimensional sonic anemometer with a fine wire thermocouple ($12.7 \mu\text{m}$) and a CSI krypton hygrometer (KH20). Air temperature, humidity and vertical wind speed were sampled at 5 Hz and covariances determined over a 15-min averaging period. Flux corrections were made for oxygen absorption by the sensor and air density effects (Webb et al., 1980, Tanner and Greene, 1989; Tanner et al., 1993). In addition net all-wave radiation, wind speed, wind direction, relative humidity, and air temperature were measured at each site. All non-turbulent parameters were sampled at 0.2 Hz and averaged over 15 min intervals. CSI 21X microloggers were used to sample and process all sensor outputs.

Instruments were mounted at 1.3 m at the WR site and at 1.8 m at the DR site. At the SU site the radiative and turbulent flux sensors were mounted at 28.5 m, and the remaining instruments at 9 m. The instruments were installed over three days SU: 91/231 (August 19, 1991), DR: 91/232 and WR: 91/233. The measurements at all sites were continuous through until 91/241 (August 31, 1991) except for a six-hour period on 91/236 when irrigation occurred at the WR site. All times are Pacific Daylight Time.

Radiosonde ascents were conducted on six days. The free flying radiosondes (AIR 'airsondes' model 3A-AS-1A) were attached to helium-filled meteorological balloons and released from the SU site at varying intervals over the day (Table I). The radiosonde sensor packages measure and transmit wet and dry bulb temperatures and ambient pressure at 10 s intervals. These were converted to potential temperature and mixing ratio in real-time by the ground-based receiver. A tracking theodolite was used to measure balloon elevation and azimuth angles at 10 s intervals, enabling layer-averaged wind speed and direction to be computed on-line. Prior to its release, each of the radiosondes was compared with an aspirated psychrometer.

TABLE I

Times of airsonde releases and the observed Bowen ratio determined from the eddy correlation measurements for the period between flights.

Day	Number of flights	Flight times (PDT)	Bowen ratio (WR)	Bowen ratio (DR)	Bowen ratio (SU)
234	3	0650, 1307, 1732	0.23	68.24	1.33
235	2	0715,1523	0.37	7.41	1.07
236	3	0647,1143,1645	Not available	12.28	0.84
238	3	0642, 1132, 1508	0.34	12.00	1.74
239	3	0640,0916,1446	0.51	10.23	1.77
240	6	0640,0805,0940,1138,1502,1701	0.31	8.34	1.50

5. Surface Heterogeneity and CBL Structure

5.1. SPATIAL REPRESENTATIVENESS OF SURFACE FLUX MEASUREMENTS

Schmid and Oke (1992) illustrate, at least for one city (Vancouver, Canada), that an average suburban block contained all the important elements to form a characteristic local suburban climate. To account for edge effects and advection, they suggest that a quasi-homogeneous region is formed if there are approximately 10 or more such units in each direction. Thus the source area needs to extend about 2 km upwind of the measurement location to achieve a representative turbulent flux.

Calculations using the flux source area model (FSAM) of Schmid (1994, 1997) indicate that during the middle of the day the turbulent flux measurements at the SU site have footprints of order 150–200 m in length and 200 m wide (Figure 4). These are representative of a neighbourhood within suburban land use. The predominant planimetric land cover within the source areas, determined by overlaying FSAM source weight functions over a georeferenced database (Grimmond 1996), are buildings and grass, with the exact fractions varying depending on the atmospheric conditions (Figure 4b). Compared to the other days, the flux source area on 91/235 contained a lower proportion of buildings, and a higher proportion of grass and water surfaces. Days 91/236, 238 and 239 show very little diurnal variation in the composition of the source area in contrast to 91/234, 235 and 240.

The fetch, i.e., the spatial extent of homogeneous land cover upwind and downwind of the turbulence sensors, at the two rural sites was over 500 m. This is much greater than the length the source areas calculated using FSAM, which are, for both sites, of order 100 m during daytime convective conditions (Schmid, 1997). Each surface type is typical of most of the land use in the Sacramento region.

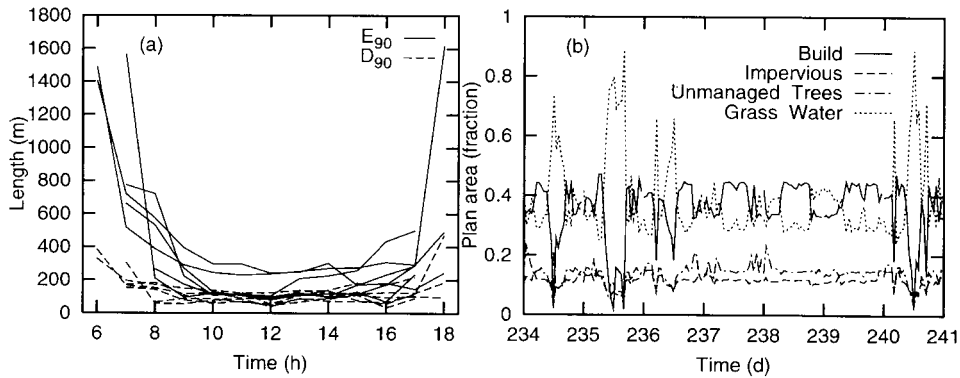


Figure 4. Dimensions of turbulent footprints calculated using the Schmid (1994, 1997) FSAM model for SU site during observation periods of CBL: (a) Length (E) and half width (D) of the 90% source area for each hour of the days when balloons were released (see Table I for times); (b) planimetric fraction of the source area comprising buildings, impervious surfaces (roads, pavement, etc.), trees and unmanaged scrub, grass and water.

5.2. REGIONAL LAND USE

For the CBL measurements, there are a number of source area dimensions to consider. Recalling Equation (7), both dS/dt (where S is θ or q) and the fluxes inferred from a DCBL approach, have a source area of ca. 100 km^2 while flux estimates from ICBL methods will have source areas of $500\text{--}1000 \text{ km}^2$ (from Equation (8)). Figure 5 illustrates the temporal variation of each of these source area dimensions using our CBL measurements. Initial estimates of the DCBL source areas were estimated from Equation (7) for the time of the sonde ascent, using the nearest 15 min average measure of F_{HO} , U (extrapolated from the surface to a mid-CBL value) together with z_i and θ estimated from the measured CBL sonde profile. Values of z_i and θ were interpolated at 2 h intervals from the measured CBL profiles to include some temporal resolution into Figure 5. These DCBL source area estimates are intended as order of magnitude estimates only, for comparison with those estimated for the ICBL method, which are calculated using Equation (8) and the average CBL windspeed measured during the integration period and the integration period (t). The key point in Figure 5 is that the two source areas differ by two to three orders of magnitude.

Two sources of data were used to classify the land cover for the Sacramento region and thus within the calculated source areas. The urban limits were identified from the USGS (United States Geological Service) 1:250,000 land use and land cover database (http://edcwww.cr.usgs.gov/glis/hyper/guide/1_250lulc, January 23, 1998). A composite Landsat-TM image was obtained for the Great Valley Region of California (http://www.biogeog.ucsb.edu/projects/gap/gap_data.html, February 05, 1998). This image is a mosaic for summer (1990) and has been resampled at 100 m. The normalised difference vegetation index (NDVI) was used to discrim-

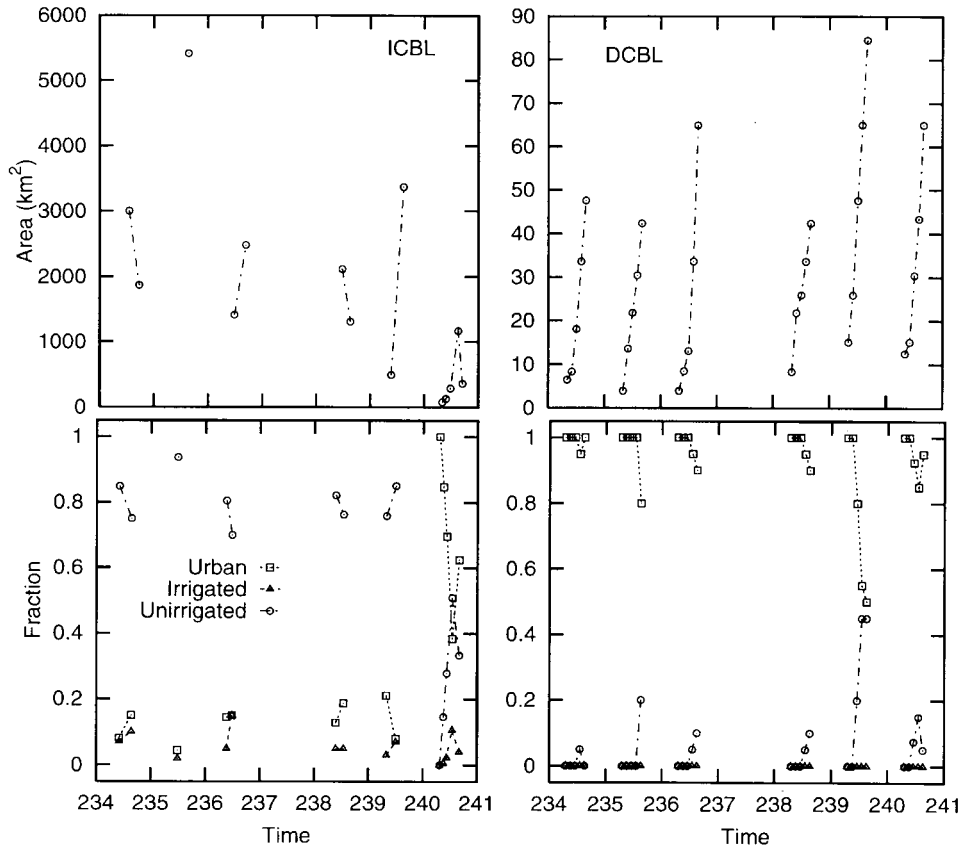


Figure 5. Calculated source areas for the ICBL and DCBL budget methods.

inate between irrigated and non-irrigated land use in the region outside the urban boundary of Sacramento. The NDVI is ideally suited to this task as it is an index of biological activity. In a typical Sacramento summer, actively growing and assimilating vegetation will be found only in irrigated fields. NDVI values greater than 0.6 were defined as irrigated, while $NDVI < 0.6$ was designated as non-irrigated (D. Graetz, personal communication). The rural area close to Sacramento, from the predominant wind directions observed in this study, is largely non-irrigated (Figure 3).

The calculated ICBL source areas were assumed to be rectangular with the length dimension 1.5 times the width. The predominant land use fraction is non-irrigated rural on all days except for 91/240 when the source areas are smaller, and thus mostly urban. This arises because of the smaller time interval between flights (Table I, Figure 5).

The DCBL source areas, calculated as described above at the time of the sonde release, were predominantly urban. It is only later in the day when z_i becomes larger, and thus the source area becomes larger, that small fractions of non-irrigated

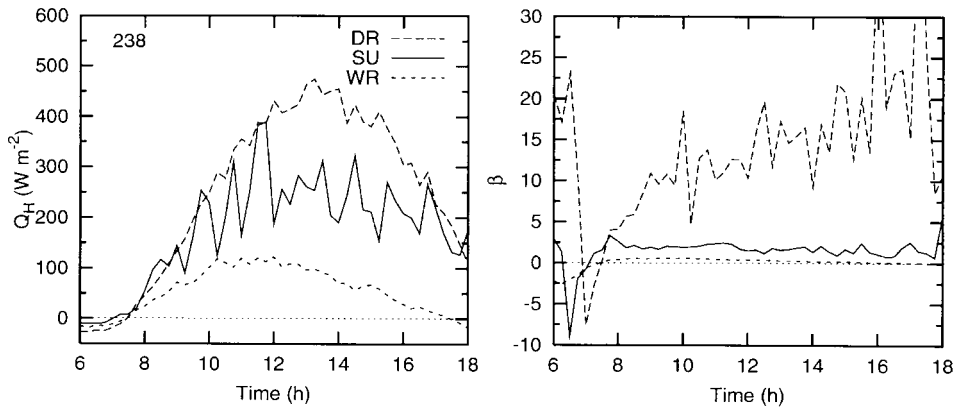


Figure 6. Diurnal variation of measured (a) Q_H and (b) ensemble Bowen ratio for each site: wet rural (WR); dry rural (DR) and suburban (SU) on 91/238.

land use are incorporated. A sensitivity test of the effect of shape of the source area, varying the length:width ratio (from 1.5 to 2), resulted in very small differences in the areal fractions of land use and is not considered further here.

5.3. MEASURED SURFACE ENERGY EXCHANGES AND CBL PROFILES

A full description and interpretation of the radiative and heat fluxes can be found in Grimmond et al. (1993) and Grimmond and Oke (1995). The SU heat and water vapour fluxes show greater variability between 15 min periods (Figure 6) and between days than the two rural sites. The observed energy fluxes at each of the three sites reveal partitioning that is typical of the respective land uses. The daytime SU sensible heat fluxes are bracketed by the larger DR and smaller WR fluxes. These features can be seen in the Figure 6a, showing the diurnal variation of the sensible heat flux for 91/238, and Figure 6b, showing the diurnal variation of the Bowen ratio. Full energy balance figures for the entire observation period are given in Grimmond et al. (1993) and Grimmond and Oke (1995). The Bowen ratio (Q_H/Q_E) at each site shows some variability from day to day, but the same relative partitioning is maintained (Table I). The Bowen ratios, as expected, are very large for the dry rural site, around unity for the suburban site, and close to those expected with equilibrium evaporation for the wet rural site.

The measured profiles of temperature and humidity, and their diurnal evolution over each day, are presented in Figure 7. In general, the temperature structure matches the slab model well. With the exception of 91/235, the γ_θ profiles above z_i are constant throughout the day. The CBL does not grow particularly deep, reaching a maximum of only 800–1000 m. The diurnal development of the temperature profiles shows that on most mornings the CBL was already approaching a well-mixed state, i.e., the nocturnal radiation inversion has been eroded, by the time of the first profile (ca. 0630 PDT). This is not the case for 91/236, where the noc-

turnal radiation inversion is still evident at 0647. All vertical temperature profiles have 2 sections: (a) a layer where the potential temperature increases rapidly with height indicating a strong temperature inversion up to about 1000 m, and (b) a layer above 1500 m where the inversion strength is less. This strong temperature inversion at around 1000 m appears to limit CBL growth. The temperature gradient in both these sections appears quite constant within each day of measurement. In the morning, the CBL temperature profiles do not show large temperature ‘jumps’ (i.e., $\Delta\theta$) at z_i . However, by mid afternoon, when convection and sensible heat flux peak, $\Delta\theta$ is more obvious.

While there is a good match between the measured temperature profiles and the structure assumed by the slab model, this is not the case for humidity. The humidity profiles show a reasonably well-mixed layer in all but the initial profile on 91/236 and 91/239. All the profiles reveal a much drier layer overlying this well-mixed layer. The humidity profiles in this drier layer overlying the CBL are complex, with a sequence of relatively moist layers that can persist over the day (see 91/239 and 240). This complex vertical humidity structure is certainly not well described by the simple slab model.

The vertical structure of the mean wind shows that the speeds are, for the most part, uniform and light ($< 5 \text{ m s}^{-1}$) throughout the well-mixed layer but there is clear wind shear in several of the early morning (0630 PDT) and mid-morning (91/239–0930 PDT) profiles. The CBL winds on 91/240 were also quite variable – both vertically and over the course of the day.

Fluxes estimated from the CBL budget method will be in error at those times when the CBL structure does not match the slab model. A check on the consistency of γ_θ over the course of each day reveals that synoptic scale advection may influence CBL warming on 91/235, where there was also a notable shift in wind direction over the day, from westerly to easterly. All other profiles showed consistent values for γ_θ throughout each day. On 91/240, the wind, temperature and humidity profiles suggest either an advective influence or some form of synoptic scale instability, which may have resulted from the cold front that moved through the Sacramento region during this day. The mixing ratio profiles were very complex with a marked humidity inversion at around 2100 m, which disappeared from the profile by 1515 PDT.

6. Predicting CBL Depth, Temperature and Humidity Using the Slab Model

The slab model was run for the six days on which radiosondes were released (Table I). The input variables (Table II) were obtained from analyses of the radiosonde profile data. Splines or Lowess fits were put through each θ and q profile to provide data at approximately 15–25 m intervals. These data were used to determine the slopes γ_θ and γ_q in addition to the values of θ and q in the mixed layer. CBL depth (z_i) was estimated by visual inspection.

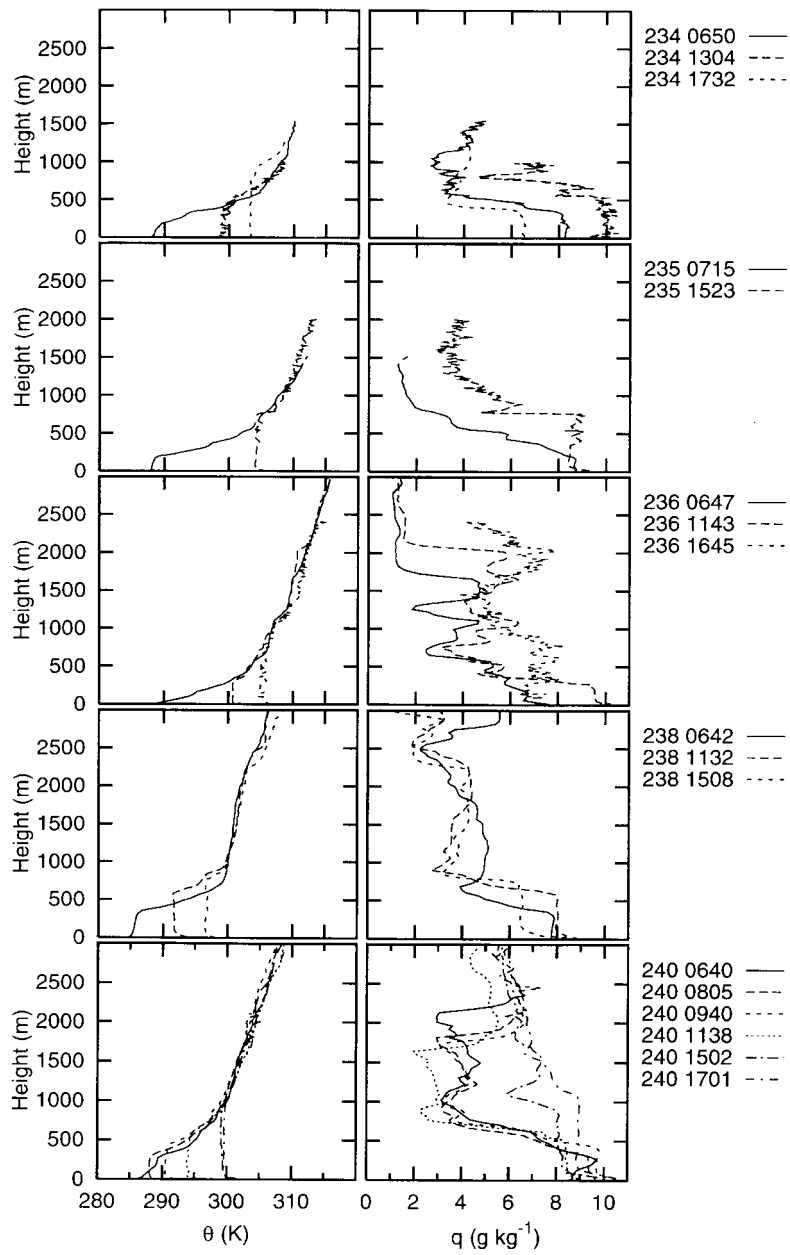


Figure 7. Corrected potential temperature and humidity profiles: diurnal evolution for each day of measurements, except 91/239 which is illustrated in Figure 1.

TABLE II
Inputs to the slab model.

Variable	Definition
<i>Surface observations at weather station</i>	
T	Temperature
q	Specific humidity
U	Wind speed
Q_H	Sensible heat flux
Q_E	Latent heat flux
P	Pressure
<i>Airsonde data</i>	
γ_θ	Slope of temperature profile with height ($d\theta/dz$)
γ_q	Slope of humidity profile with height (dq/dz)
$z_i(0)$	Initial mixed-layer depth
$\gamma_{\theta(0)}, \gamma_{q(0)}$	$d\theta/dz, dq/dz$ just above $z_i(0)$
$\theta_+(0), q_+(0)$	θ, q at just above $z_i(0)$
$\theta_m(0), q_m(0)$	Average θ, q from surface to $z_i(0)$
<i>Surface parameters</i>	
z_0	Roughness length
z_d	Zero-plane displacement length

Here we consider the performance of the model with four different CBL growth schemes [Tennekes (1973, T), Tennekes and Driedonks (1981, D), McNaughton and Spriggs (1986, M), and Rayner and Watson (1991, R)] (Equations (3a–d)). In each case performance is evaluated in terms of the mean departure of the modelled value from that observed for a particular time period (i) for three variables within the CBL: mixed-layer height (z_i), potential temperature (θ_m), and humidity (q_m). In the case of θ_m , the equation for the difference between observed and modelled data is:

$$\overline{\Delta\theta_m} = \frac{\sum_{i=1}^n |\theta_{m \text{ obs}_i} - \theta_{m \text{ mod}_i}|}{n}, \quad (9)$$

where n is the total number of profiles in the sample. Perfect correspondence would yield a mean deviation of zero and range of zero. The observed data (obs) used in this evaluation are the 14 airsonde temperature and humidity profiles ($n = 14$) collected in our field campaign, which were *not* used to initialise the model (Table I). The modelled data (mod) are the data for the 15-min period (see discussion below) closest to the radiosonde release. We have chosen to use this average difference between measured and modelled values, rather than the RMSE, to quantify the

model performance for two reasons. Firstly, the average difference retains the sign and, secondly, occasional outlying points were found to strongly bias the RMSE. Furthermore, the *magnitude* of the modelled-observed differences is very similar using both approaches and so the conclusions drawn are equally valid. The maximum and minimum differences are always included, in addition to the mean, in any presentation of modelled vs. measured performance.

6.0.1. *Initialisation of the Models*

The initialisation data for the model runs were obtained from the first airsonde release each day. The surface data used were collected at the SU site. Urban turbulent fluxes are typically averaged over periods longer than the 15 min averaging time used at the rural sites, because of the large variability mentioned above and evident in Figure 6. Typical averaging times used are of the order of 60 min (Oke et al., 1989). Although we initially evaluated the CBL model using 60 min averaged data; model performance was significantly improved by using 15 min input data. The modelled data reported here are the data for the 15 min period closest to the balloon release.

Using data for the shorter (15 min) time step highlighted the importance of the timing of model initialisation. In the field, the initial balloon releases were timed to coincide with the onset of positive sensible heat fluxes and the initiation of CBL growth. Convective heat fluxes are very small at this time and may oscillate between being positive and negative (Figure 6). The best overall performance was obtained when the model was initialised with the 15 min data when Q_H became greater than zero after 0500 h in the morning.

6.0.2. *Performance and Sensitivity to Input Parameters*

Apart from α_3 , which was varied from 0.1–0.9, the constants used in the CBL growth equations (i.e., Equations (3a)–(3d)) are the values commonly used in the literature, viz. $\alpha_1 = 0.2$, $\alpha_2 = 5$, $\alpha_4 = 0.18$, $\alpha_5 = 1.33$, and $\alpha_6 = 0.80$. In the following discussion the models are evaluated initially by forcing them with the sensible and latent heat fluxes observed at the SU site.

Figure 8a shows the performance of all four entrainment schemes by plotting z_i , $\Delta\theta_m$ and Δq_m (as defined in Equation (9)). Some schemes (Tennekes and Driedonks, D, and Rayner and Watson, R) require estimates of u_* , which was not measured directly in this study. It has been calculated from observed wind speed at 9 m, and roughness length (z_0) and zero-plane displacement length (z_d) based on the surface morphometry of the SU site using the methods of Bottema (b) (1995) and Raupach (r) (1992, 1994, 1995) (Grimmond and Oke, 1999). Stability corrections are included in the u_* calculation by iteratively solving for Obukhov length using measured Q_H and the method outlined in Grimmond and Cleugh (1994).

On average, all four models underpredict z_i and θ_m , and overpredict q_m (Figure 8a). The best performance is found using the Tennekes and Driedonks (D) en-

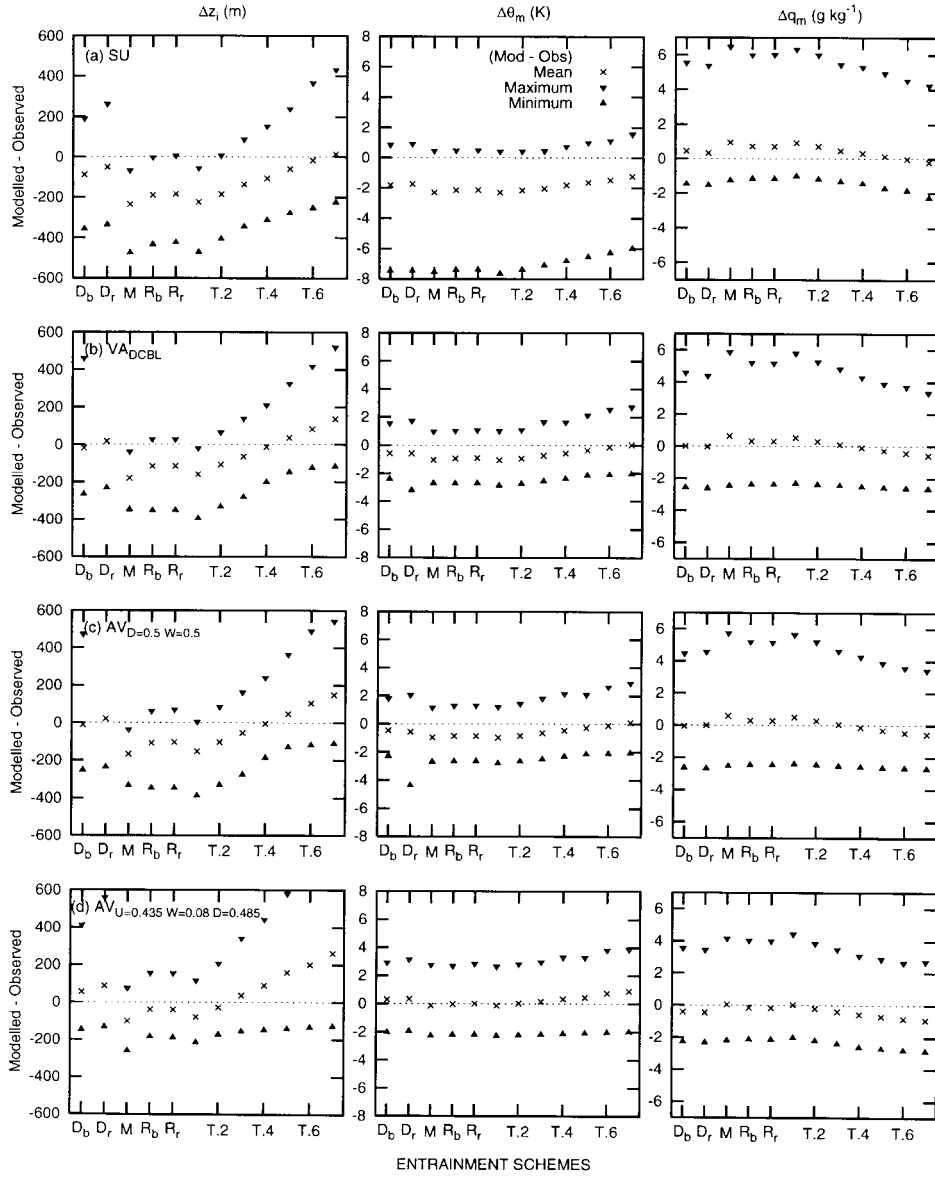


Figure 8. Evaluation of entrainment schemes and surface roughness schemes. Each plot shows mean, maximum and minimum [modelled – observed] values of z_i , θ_m and q_m for the 14 profiles using equation (9). Symbols on x-axis are: D, Tennekes and Driedonks (1981) with z_0 , z_d from b – Bottema and r – Raupach; M, McNaughton and Spriggs (1986); R, Rayner and Watson (1991); T, Tennekes (1973) with θ varying from 0.1 (T.1) – 0.9 (T.9). Panels (a)–(d) are model results using different forcing surface fluxes: (a) Q_{HS} and Q_{ES} measured at SU site; (b), (c), and (d) use a regionally-averaged Q_{HR} and Q_{ER} calculated with different weighting functions as explained in detail the text: VA_{DCBL} = weighted average surface flux calculated using fraction of surface cover in DCBL source area, from Equation (7). $AV_{D=0.5, W=0.5}$ = average surface fluxes calculated using 50% Q_H (DR) + 50% Q_H (WR). $AV_{U=0.43, D=0.485, W=0.05}$ = average surface fluxes calculated using 43% Q_H (SU) + 48% Q_H (DR) + 5% Q_H (WR).

trainment model, which does not require any additional parameters to be assigned a priori and takes into account mechanical convection via u_* . The model shows slightly improved performance for z_i and q_m when z_0 and z_d values are determined from Raupach's method.

The next best performance was obtained with the Tennekes model (T) (Figure 8a). For initial comparisons α_3 was set to 0.5 (T.5) based on the findings of Cleugh et al. (1997). As α_3 increases, the mean $\overline{\Delta z_i}$ decreases in absolute terms – this is seen in the upward trend in $\overline{\Delta z_i}$ as α_3 is increased above 0.5 in Figure 8. $\overline{\Delta z_i}$ is smallest when α_3 is set to 0.6–0.7. $\overline{\Delta \theta_m}$ also decreases with increasing α_3 , but does not reduce to zero even at $\alpha_3 > 0.9$. $\overline{\Delta q_m}$ increases with increasing α_3 , and has its absolute minimum at 0.6.

The Rayner and Watson model (R) also uses u_* but is not as sensitive to the changes in values of z_0 and z_d (Figure 8a). The poorest performance overall was found using the McNaughton and Spriggs (1986) encroachment model.

The superior performance of the entrainment schemes in terms of modelling CBL depth, particularly those that include the effects of wind shear, illustrates the importance of entrainment – especially in a landscape where the surface sensible heat flux was not very high. Chen and Oke (1994) found that the sea-breeze circulation, with a low-level landward flow and upper-level return flow, generated strong wind shear, mechanical mixing and enhanced entrainment at the top of the CBL above a coastal city. In their study, entrainment as a result of wind shear often exceeded entrainment due to buoyancy, as reflected by the improved predictions of CBL growth when larger α_3 values (0.44–0.63) were used, essentially parameterising the effect of mechanical turbulence. In this study, the contribution of shear at the top of the CBL is not incorporated in the entrainment schemes. Rather, the role of mechanical turbulence in entrainment is parameterised using a surface measure of u_* .

In contrast, θ_m and q_m predictions are not very sensitive to the choice of entrainment scheme (Figure 8a); a finding consistent with other authors (Driedonks, 1980). Average differences in q_m are very small, about 0.5–1 g kg⁻¹, regardless of the entrainment model used. Measured and modelled θ_m differ on average by 2 °C and the choice of entrainment scheme is not critical. Clearly, the choice of entrainment scheme is less important for scalar concentrations than for z_i predictions. Given that neither the D (Tennekes and Driedonks) or R (Rayner and Watson) models require α_3 to be selected a priori, they are the recommended entrainment schemes.

6.0.3. *Optimising Model Performance by Using a Regionally-Averaged Heat Flux*

Optimising the model performance using the Tennekes entrainment model, and varying α_3 as described above, reveals that model performance can be improved by increasing the flux of sensible heat (increasing α_3 does this by increasing the downward flux of sensible heat at z_i). The value of α_3 required to obtain model

agreement is, however, unrealistic – raising the question of whether the CBL source area is, in fact, much larger than the turbulent flux ‘footprint’ at the SU site. Subsidence or CBL scale advection could have a similar effect on the model performance, i.e., including either of these processes can result in increased CBL warming and growth. However, we found that an increase in surface heat flux was needed to improve the model performance, in terms of all CBL properties, on those days when there was no apparent subsidence or CBL scale advection. Furthermore, even on days when we suspect that subsidence or advection may have occurred (days 91/235 and 240), adding in a subsidence velocity did not simultaneously improve z_i , θ and q . We thus conclude that there is no evidence that the under-prediction of z_i and θ is the result of large-scale advection or subsidence.

To investigate whether the appropriate surface heat and water vapour fluxes are indeed averaged over a larger area, we force the slab model with sensible and latent heat fluxes that represent different source areas and thus surface types. Here we consider (1) the DR (dry rural) fluxes alone; (2) a composite of the DR, WR (wet rural) and SU fluxes, based on the relative fractions of each of these land use types in the CBL source area (Section 5.2); and (3) the average of the rural heat fluxes alone (i.e., DR and WR). The results reveal that when only the DR fluxes are used, the slab model overpredicts z_i and θ , and underpredicts q for all CBL growth schemes. In fact, the best performance is not achieved by using any one of these land use types alone, but rather by using a heat flux that is some average of the three land uses in the region surrounding Sacramento. This ‘regionally averaged’ heat flux is given the symbol Q_{HR} and can be defined in several ways but here we just explore the second and third options listed above (Figure 8b, c).

Figure 8b shows the model’s performance using source area dimensions calculated from Equation (7) and the actual meteorology observed for each 15 min simulation period – this means that the source area dimensions vary through time. The regional sensible and latent heat fluxes, Q_{HR} and Q_{ER} , are then computed from the weighted average of the DR, WR and SU sites, where the weighting is determined by the fraction of each of these land use types in the calculated source region. While the model performance is adequate, it is not greatly improved over the simulations using the suburban fluxes alone, as can be seen by comparing Figures 8a and 8b. A much greater improvement in model performance can be achieved using the simple weighting scheme of $Q_{HR} = 50\% Q_H(\text{DR}) + 50\% Q_H(\text{WR})$ (and similarly for Q_{ER}), as illustrated by comparing Figure 8c with Figures 8a, b.

This finding is further confirmed by Figure 8d, which illustrates the model performance using the Q_{HR} (and Q_{ER}) that yields the smallest mean differences between observed and modelled z_i , θ_m and q_m . The optimum weighting for Q_{HR} (and Q_{ER}) is 43.5% $Q_H(\text{SU})$, 48.5% $Q_H(\text{DR})$ and 8% $Q_H(\text{WR})$. This result is at odds with the DCBL source area calculations, which point to most of the flux source area for $d\theta/dt$ and dq/dt being within the Sacramento urban area. For the predominant wind directions at the study site, these optimum land use fractions oc-

cur with source area dimensions of approximately $30\text{--}35 \times 20\text{--}23$ km (assuming a length: width 1.5:1). These lengths are approximately three to five times the DCBL estimates and of a similar size to the ICBL source area dimensions.

6.0.4. Performance of Slab Model

Based on model runs using the entrainment scheme of Tennekes and Driedonks (1980) with z_0 calculated using the morphometric method of Raupach (1992, 1994, 1995), we now consider in more detail the predicted diurnal variation of θ_m , q_m and z_i compared to measurements. The weighted source areas, as used in Figure 8b, are used to weight the forcing sensible and latent heat fluxes.

While the average (Figure 8) predictions of θ_m are less than those measured, the predicted diurnal pattern (Figure 9) is in excellent agreement with the measurements on all days except for 91/235, when the model underpredicts θ_m by about 5°C . Days 91/234, 236 and 238 reveal differences of about 2°C for individual profiles. The performance in predicting q_m is slightly worse, but the discrepancy for the last profile on 91/234 is almost certainly a measurement error. The increase in CBL humidity from 0647 to 1143 PDT on 91/236 is not predicted well, but this is not surprising given the complex nature of the humidity profile on this day (Figure 7).

Day 91/240 is interesting in that it illustrates the problems encountered when synoptic conditions change. The model is forced with the 0640 PDT humidity profile. As noted earlier, there is a distinct shift in upper level humidity on this day, which means that the CBL tends to humidify in the late afternoon. These changes are not predicted, in part because the slab model does not use a time-varying γ_q .

The worst predictions of z_i occur on 91/235, 91/238 (where θ_m is also modelled poorly) and 91/240. This is to be expected on 91/235 given the change in γ_θ and wind direction. The model performance is adequate on the remaining days, but does tend to underestimate z_i .

7. Estimating Regional Heat Fluxes Using Integral CBL Methods

The need to estimate $\Delta\theta$ and Δq from instantaneous sonde measurements limits the implementation of Equation (4) to infer surface fluxes using an integral CBL approach. This is because, firstly, these values are difficult to determine from a measured profile and secondly, as demonstrated by Cleugh et al. (1997), fluxes estimated from Equation (4) are very sensitive to small errors in z_i , $\Delta\theta$ and Δq . We thus chose to estimate the surface fluxes by integrating the difference between consecutive pairs (at times t_i and t_{i+1}) of CBL profile data that had been splined at 15–25 m intervals, i.e., for sensible heat:

$$\int_{t_i}^{t_{i+1}} F_H dt = \int_{z_1}^{z_2} [(\theta(z)_{t_{i+1}} - \theta(z)_{t_i})] dz. \quad (10)$$

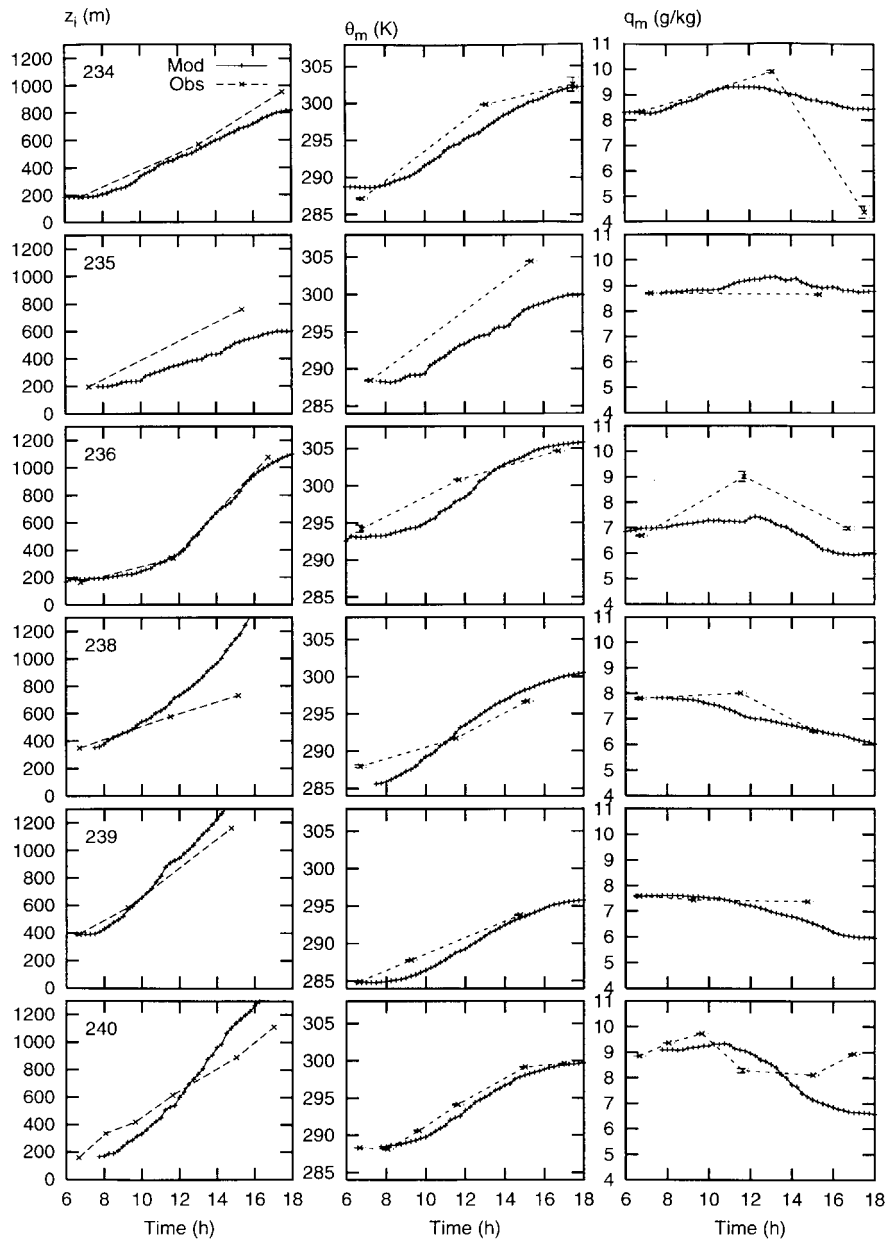


Figure 9. Measured and modelled CBL depth (z_i), potential temperature (θ_m) and specific humidity (q_m).

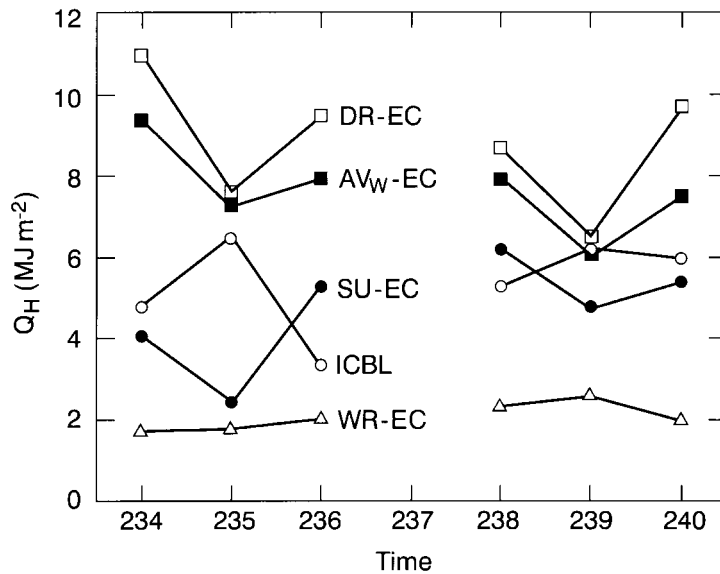


Figure 10. Total sensible heat flux determined between airsonde release times (Table I) from eddy correlation observations at SU, WR and DR. AV_W denotes 'regional' fluxes computed as an areally weighted average based on the ICBL source area.

The total integral heat flux for each of the measurement days has been computed by summing the integral heat fluxes estimated from Equation (10) and are plotted in Figure 10. Because the earliest and latest CBL profiles were measured at *ca.* 0600 and 1500 PDT, these are not daily totals. Also plotted are the total sensible heat fluxes measured at the individual flux measurement sites (SU, WR and DR) for the same time periods, and a weighted average based on the areal coverage of the land surface types derived from the NDVI and source area analysis described above (AV_W).

Although latent heat fluxes could be computed, in principle, using the same approach the poorly mixed and complex behaviour of the measured humidity profiles leads to erroneous results. As illustrated in Cleugh et al. (1997), estimates of Q_{EO} using ICBL methods are much more sensitive to errors than sensible heat flux measurements. They also found that humidity was often not well mixed through the CBL, further limiting the applicability of simple CBL budget methods for inferring latent heat fluxes. They recommend using an energy balance approach (i.e., $Q_{EO} = \text{available energy} - Q_{HO}$, where Q_{HO} is estimated from an integral CBL expression) to infer Q_{EO} from ICBL methods.

The results presented in Figure 10 are interesting. Unlike the slab modelling, where the suburban heat flux alone was insufficient to predict the measured CBL depth and temperature, the measured (local-scale) suburban heat fluxes (SU-EC in Figure 10) are similar in magnitude to the regional-scale heat fluxes determined from the ICBL approach, with the exception of day 91/235. These results also

confirm that the heat flux from the dry rural (DR) and wet rural (WR) sites alone are, respectively, much larger and smaller than the heat fluxes estimated from the ICBL method. The ICBL estimates of a regional flux, however, are probably closest to the measured regional heat flux (Q_{HR}) that has been determined by weighting Q_H from the DR, SU and WR sites according to the fractions of each land cover in the ICBL source area (AV_W). The percentage differences are within 30%, except days 234 and 236, which are typical error magnitudes for these integral CBL budget methods. The percentage differences are much larger on days 91/234 and 91/236 – 49% and 58% respectively. In fact that ICBL estimates are closer to the suburban measurements on these days. Note that on 91/236 the WR data are approximated because of the disrupted eddy correlation measurements. Finally, it is of interest to note that the entrainment fluxes estimated by integrating the area under each measured temperature profile indicate that an appropriate value for α_3 is in the range of 0.2–0.4, in agreement with the slab-model predictions described earlier.

These results suggest that the source areas for the surface fluxes inferred from the DCBL and ICBL methods are, respectively, larger and smaller than those calculated from Equations (7) and (8). In other words, regional fluxes estimated from the ICBL method seem to be a closer match to the suburban heat fluxes, while the DCBL predictions are improved by incorporating a larger percentage of the dry rural land use.

8. Discussion and Conclusions

This study explores the use of CBL budget methods to infer regionally averaged fluxes in a landscape that has, at least, three types of land cover (irrigated and non-irrigated rural and urban). The surface energy balance measurements show distinct flux partitioning for each of these dominant surface types.

We have found that the measured profiles of temperature, especially, and humidity match the structure expected for a well-mixed convective boundary layer. It is not surprising, therefore, that the predictions of CBL depth, temperature and humidity using the slab model (Equations (1)–(3)) agree fairly closely to the measured values. The entrainment scheme of Tennekes and Driedonks (1981) gives the best performance over the conditions considered here.

Improved agreement between measured and modelled CBL properties could be achieved by forcing the slab model with surface fluxes that differed from the locally measured fluxes at the suburban site (Q_{HS} and Q_{ES}). In other words, the measured CBL depth, temperature and humidity do not seem to match the input of heat and water vapour from the underlying suburban surface. Differences between measured and modelled z_i , θ and q can be minimised by forcing the slab model with regional heat (Q_{HR}) and water vapour (Q_{ER}) fluxes that are some ‘average’ of the local suburban, dry rural and wet rural heat fluxes. The optimum weighting found for Q_{HR} and Q_{ER} is 48.5% DR, 43.5% SU and 8% WR. These surface char-

acteristics are more consistent with the source area being larger than that predicted from Equation (7). This would mean that the time scale of adjustment in the CBL exceeds four eddy turnover times.

Scalar concentrations in the CBL appear to be influenced by sources both within and outside the Sacramento urban area. Correct predictions of the CBL depth, temperature and humidity, and presumably other scalar concentrations, needs to include the input of heat, water and scalars from both urban and non-urban sources. Given that simple slab models of the type used in this study are widely used for air pollution applications, this finding points to the need to correctly parameterise the regionally averaged surface heat flux. For cities like Sacramento, whose spatial extent is of order 50 km, this 'region' extends beyond the urban boundary. This also suggests that the urban boundary layer may not be solely influenced by the underlying city.

In contrast, the regional heat flux estimated from the ICBL method agrees reasonably well with regional heat fluxes calculated by appropriately weighting the measured, local scale heat fluxes for each land use type in the source area (using Equation (8)). In short, the source areas for both the DCBL and ICBL estimates seem much more similar than expected. This may, of course, be a fortuitous result that arises from the relative similarity between the urban and predominantly unirrigated rural land uses such that the average 'urban' heat flux simply matches the average Q_{HR} described above. In cases where the urban land use has a quite different surface energy balance, the ICBL and DCBL methods may yield different answers. Nonetheless, the satisfactory agreement between the heat fluxes estimated from the ICBL method, and both an estimated regional heat flux, is further evidence that this integral method provides an adequate estimate of areally averaged heat fluxes.

Acknowledgements

This work was completed while CSBG was visiting CSIRO. We gratefully acknowledge Charles Peck Elementary School; Sierra Sod and Supply and the Ingram family for their permission to locate the sites on their property. Thanks to Dr. Hans Peter Schmid for assistance with the FSAM model, Dr. Dean Graetz for assistance with the NDVI calculations, and Drs. John Finnigan and Tom Denmead for comments on a draft of this manuscript. Aspects of this work were supported by funding from USDA Forest Service Co-operative research grants (CSBG) and Indiana University (CSBG); and the Australian Research Council (HC) and Macquarie University (HC).

References

- Barr, A. G. and Betts, A. K.:1997, 'Radiosonde Boundary Layer Budgets above a Boreal Forest', *J. Geophys. Res.* **102**(D24), 29,205–29,212.
- Barr, A. G., Betts, A. K., Desjardins, R. L., and McPherson, J. I.: 1997, 'Comparison of Regional Surface Fluxes from Boundary Layer Budgets and Aircraft Measurements above Boreal Forest', *J. Geophys. Res.* **102**(D24), 29,213–29,218.
- Betts, A. K. and Ball, J. H.:1994, 'Budget Analysis of FIFE 1987 Sonde Data', *J. Geophys. Res.* **99**, 3655–3666.
- Bottema, M.:1995, 'Aerodynamic Roughness Parameters for Homogeneous Building Groups – Part 2: Results'. Document SUB-MESO #23, Ecole Centrale de Nantes, France, 80 pp.
- Briggs, G. A.: 1988, 'Surface Inhomogeneity Effects on Convective Diffusion', *Boundary-Layer Meteorol.* **45**, 117–135.
- Brutsaert, W. and Mawdsley, J. A.: 1976, 'The Applicability of Planetary Boundary Layer Theory to Calculate Regional Evapotranspiration', *Water Resour. Res.* **12**, 852–857.
- Ching, J. K. S.:1985, 'Urban Scale Variations of Turbulence Parameters and Fluxes', *Boundary-Layer Meteorol.* **33**, 336–361.
- Cleugh, H. A.: 1991, 'Predicting Catchment Scale Evaporation Using a Coupled Boundary Layer Growth/Canopy Evaporation Model', *Vegetatio* **9**, 135–148.
- Cleugh, H. A. and Grimmond, C. S. B.: 1993, 'A Comparison between Measurements of Local-Scale "Suburban" and Areal-Averaged "Urban" Heat and Water Vapour Fluxes. Exchange Processes at the Land Surface for a Range of Space and Time Scales', *International Association of Hydrological Sciences Publication* **212**, 155–163.
- Cleugh, H. A., Briggs, P. R., and Raupach, M. R.: 1997, 'CBL Budget Estimates of Regional Scale Energy and Water Vapour Fluxes during OASIS', in D. Jasper and T. Beer (eds.), *Abstracts: IAMAS and IAPSO 1997 Joint Assemblies, Melbourne, Australia, 1–9 July 1997*. IAMAS-IAPSO Organising Committee, Melbourne, Australia, Abstract IM13YY.
- Cooper, D. I. and Eichinger, W. E.: 1994, 'Structure of the Atmosphere in an Urban Planetary Boundary Layer from Lidar and Radiosonde Observations', *J. Geophys. Res.* **99**(D11), 22,937–22,948.
- Culf, A. D.: 1992, 'An Application of Simple Models to Sahelian Convective Boundary-Layer Growth', *Boundary-Layer Meteorol.* **58**, 1–18.
- Denmead, O. T., Raupach, M. R., Dunin, F. X., Cleugh, H. A., and Leuning, R.: 1996, 'Boundary-Layer Budgets for Regional Estimates of Scalar Fluxes', *Global Change Biol.* **2**, 255–264.
- Driedonks, A. G. M.: 1982, 'Models and Observations of the Growth of the Atmospheric Boundary Layer', *Boundary-Layer Meteorol.* **23**, 283–306.
- Godowitch, J. M., Ching, J. K. S., and Clarke, J. F.: 1987, 'Spatial Variation of the Evolution and Structure of the Urban Boundary Layer', *Boundary-Layer Meteorol.* **38**, 249–272.
- Grimmond, C. S. B.: 1996, 'Dynamically Determined Parameters for Urban Energy and Water Exchange Modelling', in M. F. Goodchild, L. T. Steyaert, B. O. Parks, C. Johnston, C. Maidment, D. Crane, and S. Glendinning (eds.), *GIS and Environmental Modeling: Progress and Research Issues*, GeoWorld, pp. 305–309.
- Grimmond, C. S. B. and Cleugh, H. A.: 1994, 'A Simple Method to Determine Obukhov Lengths for Suburban Areas', *J. Appl. Meteorol.* **33**, 435–440.
- Grimmond, C. S. B. and Oke, T. R.: 1995, 'Comparison of Heat Fluxes from Summertime Observations in the Suburbs of Four North American Cities', *J. Appl. Meteorol.* **34**, 873–889.
- Grimmond, C. S. B. and Oke, T. R.: 1999, 'Aerodynamic Properties of Urban Areas Derived from Analysis of Surface Form', *J. Appl. Meteorol.* **38**, 1262–1292.
- Grimmond, C. S. B., Oke, T. R., and Cleugh, H. A.: 1993, 'The Role of "Rural" in Comparisons of Observed Suburban–Rural Flux Differences. Exchange Processes at the Land Surface for a Range

- of Space and Time Scales', *International Association of Hydrological Sciences Publication* **212**, 165–174.
- Hildebrand, P. H. and Ackerman, B.: 1984, 'Urban Effects on the Convective Boundary Layer', *J. Atmos. Sci.* **41**, 76–91.
- Hipps, L. E., Swiatek, E., and Kustas, W. P.: 1994, 'Interactions between Regional Surface Fluxes and the Atmospheric Boundary Layer over a Heterogeneous Watershed', *Water Resour. Res.* **30**, 1387–1392.
- Horst, T. W. and Weil, J. C.: 1992, 'How Far Is Far Enough? The Fetch Requirements for Micrometeorological Measurements', *J. Atmos. Ocean. Technol.* **11**, 1018–1025.
- Leclerc, M. Y. and Thurtell, G. W.: 1990, 'Footprint Predictions of Scalar Fluxes Using a Markovian Analysis', *Boundary Layer Meteorol.* **52**, 247–258.
- Lhomme, J.-P. and Monteny, B.: 1997, 'Inferring Regional Surface Fluxes from Convective Boundary Layer Characteristics in the Sahelian Environment', *Water Resour. Res.* **33**, 2563–2569.
- McNaughton, K. G. and Spriggs, T. W.: 1986, 'A Mixed-Layer Model for Regional Evaporation', *Boundary-Layer Meteorol.* **34**, 243–263.
- Miao, Y. and Cleugh, H. A.: 1997, 'Modelling Studies of Atmospheric Boundary Layer Responses to Surface Heterogeneity', in D. Jasper and T. Beer (eds.), *Abstracts: IAMAS and IAPSO 1997 Joint Assemblies, Melbourne, Australia, 1–9 July 1997*. IAMAS-IAPSO Organising Committee, Melbourne, Australia, Abstract IM1300.
- Munley, W. G. and Hipps, L. E.: 1990, 'Estimation of Regional Evaporation for a Tall Grass Prairie from Measurements of Properties of the Atmospheric Boundary Layer', *Water Resour. Res.* **27**, 225–230.
- Oke, T. R.: 1976, 'The Distinction between Canopy and Boundary Layer Urban Heat Islands', *Atmosphere* **14**, 268–277.
- Oke, T. R. and East, C.: 1971, 'The Urban Boundary Layer in Montréal', *Boundary-Layer Meteorol.* **1**, 411–437.
- Oke T. R., Cleugh H. A., Grimmond, C. S. B., Schmid, H. P., and Roth, M.: 1989, 'Evaluation of Spatially-Averaged Fluxes of Heat, Mass and Momentum in the Urban Boundary Layer', *Wea. Clim.* **9**, 14–21.
- Pielke, R. A., Cotton, W. R., Walko, R. L., Tremback, C. J., Lyons, W. A., Grasso, L. D., Nicholls, M. E., Moran, M. D., Wesley, D. A., Lee, T. J., and Copeland, J. H.: 1992, 'A Comprehensive Meteorological Modeling System – RAMS', *Meteorol. Atmos. Phys.* **49**, 69–91.
- Raupach, M. R.: 1991, 'Vegetation-Atmosphere Interaction in Homogeneous and Heterogeneous Terrain: Some Implications of Mixed-Layer Dynamics', *Vegetatio* **9**, 105–120.
- Raupach, M. R.: 1992, 'Drag and Drag Partition on Rough Surfaces', *Boundary-Layer Meteorol.* **60**, 375–395.
- Raupach, M. R.: 1993, 'The Averaging of Surface Flux Densities in Heterogeneous Landscapes, Exchange Processes at the Land Surface for a Range of Space and Time Scales', *International Association of Hydrological Sciences Publication* **212**, 343–355.
- Raupach, M. R.: 1994, 'Simplified Expressions for Vegetation Roughness Length and Zero-Plane Displacement as Functions of Canopy Height and Area Index', *Boundary-Layer Meteorol.* **71**, 211–216.
- Raupach, M. R.: 1995, 'Corrigenda', *Boundary-Layer Meteorol.* **76**, 303–304.
- Raupach, M. R.: 2000, 'Combination Theory and Equilibrium Evaporation', *Quart. J. Roy. Meteorol. Soc.*, in press.
- Raupach, M. R., Denmead, O. T., and Dunin, F. X.: 1992, 'Challenges in Linking Atmospheric CO₂ Concentrations to Fluxes at Local and Regional Scales', *Aust. J. Bot.* **40**, 697–716.
- Rayner, K. and Watson, I. D.: 1991, 'Operational Prediction of Daytime Mixed Layer Heights for Dispersion Modelling', *Atmos. Environ.* **25A**(8), 1427–1436.
- Schmid, H. P.: 1994, 'Source Areas for Scalars and Scalar Fluxes', *Boundary-Layer Meteorol.* **67**, 293–318.

- Schmid, H. P.: 1997, 'Experimental Design for Flux Measurements: Matching Scales of Observations and Fluxes', *Agric. For. Meteorol.* **87**, 179–200.
- Schmid, H. P. and Oke, T. R.: 1990, 'A Model to Estimate Source Areas Contributing to the Turbulent Exchange in the Surface Layer over Patchy Terrain', *Quart. J. Roy. Meteorol. Soc.* **116**, 965–988.
- Schmid, H. P., and Oke, T. R.: 1992, 'Scaling North American Urban Climates by Lines, Lanes, and Rows', in D. G. Janelle (ed.), *Geographical Snapshots of North America*, The Guildford Press, New York, 442 pp.
- Tanner, B. D. and Greene, J. P.: 1989, 'Measurements of Sensible Heat and Water Vapor Fluxes Using Eddy Correlation Methods', Final Report to U.S. Army Dugway Proving Grounds, DAAD 09-87-D-0088, 94 pp.
- Tanner, B. D., Swiatek, E., and Greene, J. P. 1993, 'Density Fluctuations and Use of Krypton Hygrometers in Surface Flux Measurements', Management of Irrigation and Drainage Systems, ASCE, July 21–23, Park City, Utah, pp. 945–952.
- Tapper, N. J.: 1990, 'Urban Influences on Boundary Layer Temperature and Humidity: Results from Christchurch, New Zealand', *Atmos Environ.* **24B**, 19–27.
- Tennekes, H.: 1973, 'A Model for the Dynamics of the Inversion above a Convective Boundary Layer', *J. Atmos. Sci.* **30**, 558–567.
- Tennekes, H. and Driedonks A. G. M.: 1981, 'Basic Entrainment Equations for the Atmospheric Boundary Layer', *Boundary-Layer Meteorol.* **20**, 515–531.
- Webb, E. K., Pearman, G. J., and Leuning, R.: 1980, 'Correction of Flux Measurements for Density Effects Due to Heat and Water Vapor Transfer', *Quart. J. Roy. Meteorol. Soc.* **106**, 85–100.

